Influence of Nonaqueous Solvents on the Electrochemistry of Oxygen in the Rechargeable Lithium– Air Battery

ARTICLE *in* THE JOURNAL OF PHYSICAL CHEMISTRY C · APRIL 2010

Impact Factor: 4.77 · DOI: 10.1021/jp102019y

Influence of Nonaqueous Solvents on the Electrochemistry of Oxygen in the Rechargeable Lithium−Air Battery

Cormac O. Laoire, Sanjeev Mukerjee, and K. M. Abraham*

Department of Chemistry and Chemical Biology, Northeastern University, 360 Huntington Avenue, Boston, Massachusetts 02115

Edward J. Plichta and Mary A. Hendrickson

U.S. Army CERDEC, Army Power Division, Ft. Monmouth, New Jersey 07703

Received: March 5, 2010; Revised Manuscript Received: March 23, 2010

A fundamental study of the influence of solvents on the oxygen reduction reaction (ORR) in nonaqueous electrolytes has been carried out for elucidating the mechanism of the oxygen electrode processes in the rechargeable Li−air battery. Using either tetrabutylammonium hexafluorophosphate ($TBAPF_6$) or lithium hexafluorophosphate ($LiPF_6$) electrolyte solutions in four different solvents, namely, dimethyl sulfoxide (DMSO), acetonitrile (MeCN), dimethoxyethane (DME), and tetraethylene glycol dimethyl ether (TEGDME), possessing a range of donor numbers (DN), we have determined that the solvent and the supporting electrolyte cations in the solution act in concert to influence the nature of reduction products and their rechargeability. In solutions containing TBA^+, O_2 reduction is a highly reversible one-electron process involving the O_2/O_2^- couple. On the other hand, in Li^+-containing electrolytes relevant to the Li−air battery, O_2 reduction proceeds in a stepwise fashion to form O_2^-, O_2^{2-}, and O^{2-} as products. These reactions in the presence of Li^+ are irreversible or quasi-reversible electrochemical processes, and the solvents have significant influence on the kinetics, and reversibility or lack thereof, of the different reduction products. The stabilization of the one-electron reduction product, superoxide (O_2^-) in TBA^+ solutions in all of the solvents examined can be explained using Pearson's hard soft acid base (HSAB) theory involving the formation of the TBA^+---O_2^- complex. The HSAB theory coupled with the relative stabilities of the Li^+−$(solvent)_n$ complexes existing in the different solvents also provide an explanation for the different O_2 reduction products formed in Li^+-conducting electrolyte solutions. Reversible reduction of O_2 to long-lived superoxide in a Li^+-conducting electrolyte in DMSO has been shown for the first time here. Our results provide a rational approach to the selection of organic electrolyte solutions for use in the rechargeable Li−air battery.

1. Introduction

The nonaqueous, rechargeable Li−air battery, introduced in 1996[1] has emerged as a major candidate for future alternative energy source. It is actively being developed worldwide because of its potential to deliver ultrahigh energy density in a battery that is low cost and environmentally friendly. In the first rechargeable Li−air cell reported by Abraham,[1] composed of a Li metal anode, a polyacrylonitrile-based gel polymer electrolyte,[2−4] and a porous carbon cathode, Li_2O_2, was identified as the discharge product. The formation of Li_2O_2 is consistent with the open circuit voltage (OCV) of about 2.9 V measured for the cell (eq 1) and the theoretical voltages calculated for possible Li−air cell reactions depicted in eqs 1−3.

$$2Li + O_2 = Li_2O_2 \quad \Delta G^o = -145 \text{ kcal } (E^o = 3.1 \text{ V}) \quad (1)$$

$$4Li + O_2 = 2Li_2O \quad \Delta G^o = -268 \text{ kcal } (E^o = 2.91 \text{ V}) \quad (2)$$

$$Li + O_2 = LiO_2 \quad \Delta G^o = -70 \text{ kcal } (E^o = 3.0 \text{ V}) \quad (3)$$

Equations 1−3 reveal that two other products besides Li_2O_2 can be formed from the reduction of oxygen. Recently, we have shown[3] that the first product of the reduction of oxygen in nonaqueous electrolytes is superoxide, O_2^-, involving a one-electron process. We also found that the half-life of the superoxide depends on the nature of the supporting electrolyte cation present in the electrolyte solution. In the presence of tetrabutylammonium cations (Bu_4N^+) in acetonitrile solutions, the superoxide, Bu_4NO_2, is extremely stable and resists further reduction to O_2^{2-} or O^{2-}. On the other hand, in presence of Li^+ ions, the superoxide, LiO_2, is unstable with a very short half-life and decomposes to Li_2O_2 and O_2. The LiO_2 that survives decomposition can be reduced to Li_2O_2. The electrochemistry of O_2 in the presence of Na^+ is somewhat similar to that in the presence of Li^+, except that the NaO_2 first formed appears to decompose very rapidly to Na_2O_2. Recent data[5] suggest that Li_2O is probably formed in some Li/O_2 cells from the reduction of Li_2O_2. The rechargeable Li−air battery research is in its infancy and a lot of further work remains to be done to fully elucidate the cell chemistry involved in discharge/charge cycling, and to bring this technology to practicability. A number of research groups have heeded the call and investigated various aspects of this battery. The work so far can be divided into three major categories: (1) Li−air cells with liquid and solid electrolytes, (2) porous electrode materials and structures, and cell performance evaluation, and (3) catalysis of cell reactions

Read has contributed to liquid electrolytes[6−8] for Li−air batteries. Having conducted an exhaustive review of solvent properties, he found electrolyte formulation as having the largest

* Author to whom technical correspondence should be addressed. E-mail: kmabraham@comcast.net.

10.1021/jp102019y
Published on Web 04/12/2010

influence on cell performance, including the nature of the reduction products. Discharge capacity is dependent on O_2 solubility, which led him to suggest ether-based electrolytes for improved cell performance. Abraham et al.[2] studied low volatile organic liquid and polymer electrolytes for the Li−air battery. Hydrophobic ionic liquids[9,10] have been studied as electrolytes, demonstrating good lithium stability and high cell discharge capacities. Another avenue of investigation involved applying existing electrolytes from conventional Li-ion batteries to the Li−air[11] battery. Recently, the usefulness of solid electrolytes for Li−air batteries has been demonstrated with an all-solid-state rechargeable Li−air battery.[12] Protected lithium electrodes (PLE) stabilized by lithium ion conductors[13] have been applied successfully in both aqueous and nonaqueous Li batteries. Finally, low loading of a very high surface area carbon on nickel foam[14] has demonstrated the highest discharge capacity thus far. Since the discharge products of the Li−air battery are insoluble in most organic electrolytes, a porous electrode structure with appropriate morphology, surface structure, pore volume, and surface area is crucial for the oxygen reduction reaction (ORR) and rechargeability of the Li−air cell. Abraham et al. clearly established in their first paper[1] that the Li/O_2 cell is rechargeable. They found that, in the absence of a catalyst of pyrolyzed cobalt phthalocyanine (Co−Pc), the recharge occurs at about 4 V, with a large hysteresis between charge and discharge voltages. The hysteresis was reduced and the charge/discharge efficiency increased with the Co−Pc-based catalyst. Recent investigations have employed manganese oxide (MnO_2) catalysts[15] although the charge voltages in these cells are similar to the voltages of the uncatalyzed cells. Our recent studies have revealed that the Li/O_2 cell can be recharged with high efficiency without a catalyst using an appropriate porous carbon electrode.[3,16] Interestingly, charge voltages of these uncatalyzed cells are similar to those of the MnO_2 catalyzed cells with both of these cells exhibiting higher charge voltages than the cobalt-catalyzed cells. Clearly, a full understanding of the mechanism of the cell discharge reaction mechanism and rechargeability is still lacking.

In this paper we report on the results of a detailed study of the influence of nonaqueous solvents on O_2 electrochemistry. Our results have shown a relationship between the Lewis basicity of the solvents, measured by their Gütmann donor numbers (DN),[17] the Lewis acidity of the cations, and the relative stabilities of the oxygen reduction products in presence of TBA^+ and Li^+, and their rechargeability. These results complementing our recently published results[3] on the influence of supporting electrolyte cations on O_2 reduction products are expected to provide the ability to systematically design and select new electrolytes for the rechargeable Li−air battery.

The structural formulas of the four solvents studied and their acronyms used here are

$$(CH_3)_2S{=}O \text{ (DMSO)}$$

$$CH_3OCH_2CH_2OCH_3 \text{ (DME)}$$

$$CH_3CN \text{ (MeCN)}$$

$$CH_3O(CH_2CH_2O)_4CH_3 \text{ (TEGDME)}$$

2. Experimental Section

Materials. Anhydrous acetonitrile (MeCN), dimethyl sulfoxide (DMSO), 1,2-dimethoxyethane (DME), and Pursis tetraethylene glycol dimethyl ether (TEGDME) were purchased from Sigma-Aldrich, Allentown, PA. All chemicals were dried with Li and were stored and prepared in an MBraun drybox filled with purified argon where the moisture and oxygen content was less than 1 ppm. The dried solvents were stored over 0.3 or 0.4 nm molecular sieves, and prior to actual measurements all solvents were degassed under vacuum.

TABLE 1: Conductivity of the Electrolyte Solutions

solvent	conductivity, σ (mS/cm) Li^+	conductivity, σ (mS/cm) TBA^+
DMSO	2.11	2.08
MeCN	14.39	10.85
DME	1.16	1.42
TEGDME	0.3	0.2

Tetrabutylammonium hexafluorophosphate ($TBAPF_6$) electrochemical grade, ≥99.0% (Fluka, puriss grade) from Sigma-Aldrich, Allentown, PA, was dried under reduced pressure at room temperature. Lithium hexafluorophosphate ($LiPF_6$) (battery grade, >99.9%, H_2O < 20 ppm) was obtained from Ferro Corp., Cleveland, OH.

Electrochemical Experiments. The electrochemical experiments were performed with an Autolab (Ecochemie Inc., model-PGSTAT 30) potentiostat equipped with a bipotentiostat interface in an airtight electrochemical cell. The electrochemical cell designed and built in-house consisted of a traditional three-electrode system utilizing platinum (Pt) mesh as the reference electrode and Pt mesh as the counter electrode. This reference electrode was used because of the instability of Li foil typically used in Li^+ conducting electrolytes as a reference electrode because of its reaction in acetonitrile. The Pt reference electrode provided stable potentials and was calibrated with reference to the ferrocenium ion/ferrocene couple (Fc^+/Fc) in each electrolyte studied, which in turn was calibrated to Li/Li^+ in a stable ethylene carbonate/dimethyl carbonate-based electrolyte. The cell also had inlet and outlet valves for oxygen or argon purging. The cell was entirely airtight with the exception of the gas outlets, which were kept under pressure with the working gas. The glassy carbon (5 mm diameter) working electrode employed for the cyclic voltammetry experiments was polished with 0.5 and 0.05 mm alumina paste prior to the experiments. For RDE experiments, the glassy carbon electrode was rotated with a Pine AFCPRB RDE rotor. All of the cyclic voltammetry experiments were initially performed in an argon-atmosphere glovebox where H_2O and O_2 concentrations were kept below 1 ppm and the temperature was held at 22 ± 2 °C. For RDE experiments the cell was brought outside of the glovebox and placed in a glovebag purged with argon. The electrolyte solutions were first purged with argon, and the electrode was cycled continuously until a reproducible cyclic voltammetric profile was obtained. The solutions were then purged with O_2 for ORR measurements. The electrochemical impedance measurements were performed with the Autolab PG 30 supplied with a FRA 2 module for impedance measurements. The impedance spectra were measured in the frequency range from 100 mHz to 100 kHz at open circuit potential with an ac voltage amplitude of 5 mV. Conductivity measurements of all samples were carried out using a 4-probe Thermo Orion conductivity cell from Thermo Fisher Scientific Inc., Waltham, MA. Conductivity data for the solutions of 0.1 M NBu_4PF_6 and $LiPF_6$ in dimethyl sulfoxide (DMSO), acetonitrile (MeCN), 1,2-dimethoxyethane (DME), and tetraethylene glycol dimethyl ether (TEGDME) are summarized in Table 1. All measurements were carried out at room temperature.

TABLE 2: Solvent Properties

solvent	ε (25 °C)	DN (kcal/mol)	viscosity η (cP)	oxygen solubility (mM/cm^3)
dimethyl sulfoxide (DMSO)	48.0[a]	29.8[d]	1.948[e]	2.10[g]
acetonitrile (ACN)	36.64[a]	14.1[d]	0.361[e]	8.1[g]
tetrathylene glycol dimethyl ether	7.79[b]	16.6[d]	4.05[f]	4.43[h]
1,2-dimethoxyethane (DME)	7.2[c]	20.0[d]	0.46[d]	9.57[h]

[a] Goldfarb et al.[28] [b] Rivas et al.[29] [c] Lago et al.[30] [d] Chemistry of nonaqueous solutions.[31] [e] Aminabhavi et al.[32] [f] Marcus properties of solvents.[33] [g] Sawyer et al.[18] [h] Read.[5]

3. Oxygen Reduction Reactions in Selected Nonaqueous Electrolytes

Electrolytes based on aprotic nonaqueous solvents are the ideal medium to investigate the oxygen reduction reactions (ORR) relevant to the Li−air battery. An environment free of protons could enable the full reduction of oxygen, essential to realize the full energy density of the Li−air cell without interference from protonated intermediates or products. Our previous work[3] revealed that the three possible O_2 reduction products in the Li−air battery, LiO_2, Li_2O_2, and Li_2O are highly polar. Therefore, appropriate polar solvents are required to dissolve these products to avoid their precipitation and passivation of the electrode surface. However, there is no metric currently existing to select the optimum nonaqueous solvent for the rechargeable Li−air battery. Polar solvents such as sulfoxides ($R_2S{=}O$), ethers (R−O−R), and nitriles ($RC{\equiv}N$) are potentially useful candidates as they may dissolve O_2 reduction products at least partially to promote rechargeability, but there is no guiding principle presently available to select the best solvent or family of solvents. Table 2 lists the four solvents with widely varying properties, particularly donor numbers (DN) that are a measure of solvent basicity, investigated in this work. We have purposely chosen these solvents with the goal of identifying a fundamental property or properties that can be used as the metric to select solvents with optimum properties for the Li−air battery.

3.1. ORR in $TBAPF_6$ Solutions in DMSO, DME, and MeCN. Dimethyl sulfoxide (DMSO) is a highly polar versatile solvent, which displays high salt solubility to produce well-conducting solutions with a wide electrochemical window (Figure 1A). This figure also displays a cyclic voltammogram (CV) for the reduction of oxygen in a 0.1 M $TBAPF_6$/DMSO electrolyte. The peak potential separation ΔE_p between the anodic ($E_{pa} = 2.40$ V) and cathodic ($E_{pc} = 2.34$ V) peaks is 60 mV and the charge area ratio (Q_a/Q_c) under the peaks is close to unity. These results indicate that O_2 reduction in the presence of TBA^+ ions is reversible. Figure 2 portrays a Randles−Sevcik (RS) plot of this ORR. The Randles−Sevcik equation (4) describes the relationship between the current and scan rate of a reversible electrochemical reaction. The magnitude of the current (I) is a function of temperature, T, the oxygen concentration in solution, C (2.1 mM),[18] electrode area A, the number of electrons transferred n, the diffusion coefficient D, and the rate, V, at which the potential is scanned (scan rate).

$$I_{pa} = (2.69 \times 1.0^5)n^{3/2}AD^{1/2}V^{1/2}C \qquad (4)$$

The plot of experimental data versus a theoretical Randles−Sevcik plot shows that it is in close agreement with the $n = 1$ theoretical plot, thereby indicating that E_{pc} is a one-electron reduction process. The plot linearity also suggests that this is a mass transport limited process. This behavior is identical to that we previously found in $TBAPF_6$/acetontrile[3] and by others in $TBAClO_4$ solutions.[18] The reductions of O_2 in DME/$TBAPF_6$ and MeCN/$TBAPF_6$ exhibit similar behavior, as shown in Figure 1B, indicating the general nature of the mechanism of O_2 reduction in TBA^+-containing solutions. The O_2 reduction potential and the associated current varied slightly in the different electrolytes, probably due to the different O_2 solubilities and reduction kinetics. The voltammograms obtained from the RDE experiments were analyzed using the Levich equation (5), which defines the relationship between current at a rotating disk electrode RDE and the angular frequency (ω) of rotation of the electrode.

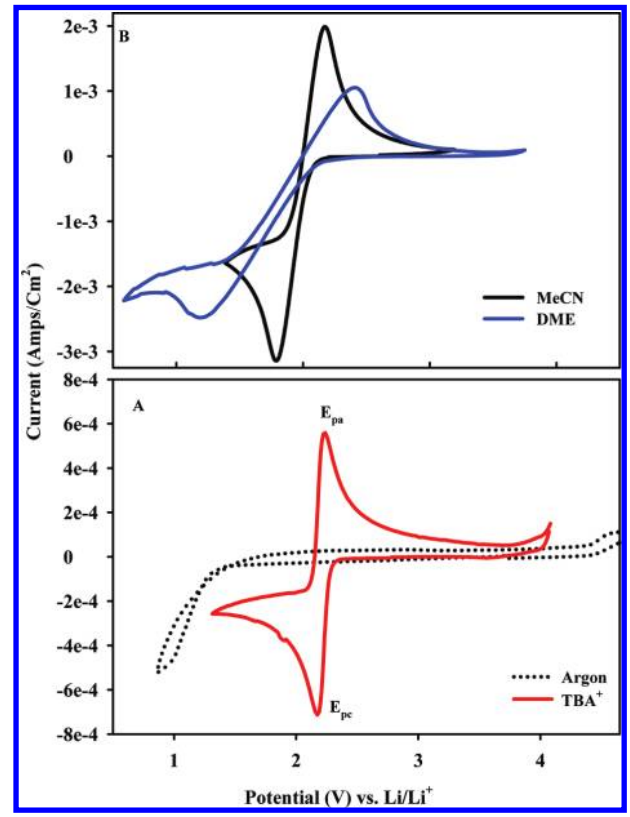

Figure 1. (A) Cyclic voltammograms for the reduction of oxygen in 0.1 M $TBAPF_6$ (red, *iR* corrected) and the argon background (dotted) in DMSO. (B) Cyclic voltammograms (*iR* uncorrected) for the reduction of oxygen in 0.1 M $TBAPF_6$/MeCN (black) and DME (blue). Scan rate 100 mV/s.

$$i_{lim} = (0.620)nFAD^{2/3}\omega^{1/2}v^{-1/6}C \qquad (5)$$

In eq 5 i_{lim} is the limiting current density (amps), n is the number of electrons involved in the reaction, F is the Faraday constant (96 500 C mol^{-1}), D is the diffusion coefficient of oxygen in the solution, and v is the kinematic viscosity of the solution (1.9×10^{-3} cm^2 s^{-1}).[19] In RDE voltammetry, the steady state is reached quickly, eliminating double layer charging. Also mass transfer effects are eliminated, as mass transfer rates are much larger than

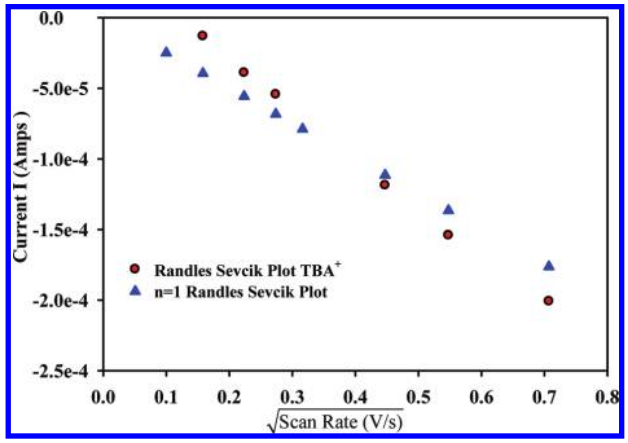

Figure 2. Randles−Sevcik plot of peak current vs square root of the scan rate in 0.1 M $TBAPF_6$/DMSO.

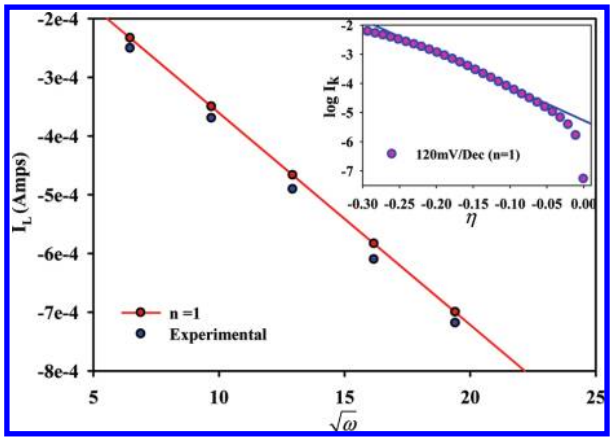

Figure 3. Levich plot of limiting current vs square root of rotation in 0.1 M $TBAPF_6$/DMSO scan rate = 100 mV s^{-1} (inset: Tafel plot).

diffusion rates allowing for accurate kinetics calculations. Figure 3 displays the Levich plot for the reduction of oxygen in 0.1 M $TBAPF_6$/DMSO; its linearity indicates that mass transfer of oxygen from the bulk solution to the electrode surface controls the limiting current. The experimental Levich plot parallels the theoretical line when $n = 1$, which is consistent with the CV data. The kinetic nature of the reaction can be further investigated using the Tafel equation,

$$\log i_k = \log i_o + \left(\frac{1 - \alpha nF}{RT}\right)\eta \tag{6}$$

A plot of log i_k versus overpotential (η) should be linear, from which the transfer coefficient α and the exchange current density i_o can be determined. The inset in Figure 3 shows cathodic Tafel plots obtained after the measured current is corrected for mass transport to give the kinetic current. The kinetic current is calculated from the equation

$$i_k = \frac{i_{lim} i}{i_{lim} - i} \tag{7}$$

where i_k is the kinetic current density, i is the measured current density during O_2 reduction, and i_{lim} is the diffusion limited current density from the Levich plot. The Tafel slope is consistent with a reversible one-electron reduction to superoxide, as the slope is very close to 120 mV dec^{-1}. This indicates that E_{pc} is the rate-

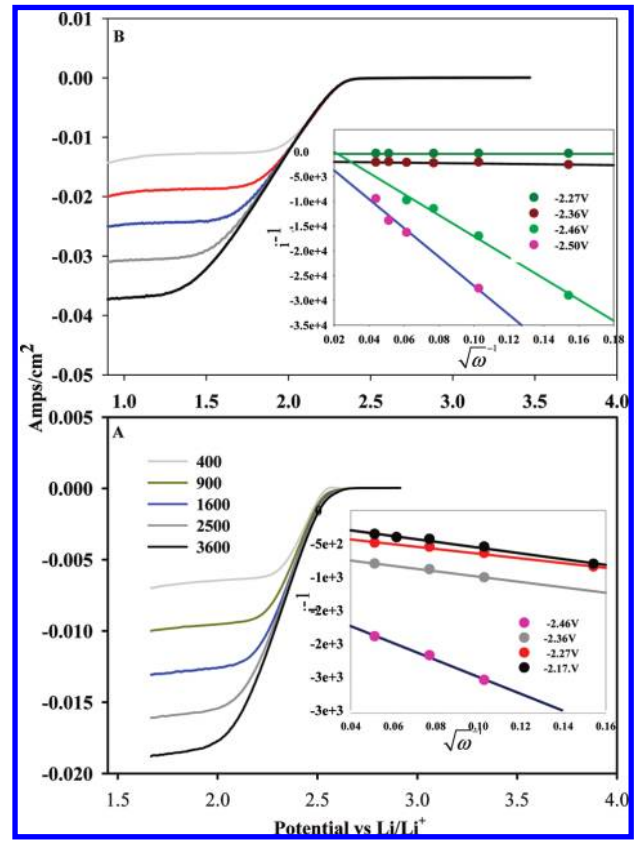

Figure 4. Current−voltage curves measured at 100 mV/s on a GC rotating disk electrode (400−3600 rpm) for oxygen reduction in (A) 0.1 M $TBAPF_6$/DMSO and (B) 0.1 M $TBAPF_6$/MeCN. Insets: Koutecky−Levich plot at different potentials in kinetic-diffusion region of the polarization curve.

determining step (rds). The reversibility of this step is evident from the kinetic data listed in Table 5. The kinetic current density, i_k, the diffusion-limited current i_{lim} density, and the measured current density, i, are related through the Koutecky−Levich equation

$$\frac{1}{i} = \frac{1}{iK} + \frac{1}{i\text{lim}} = \frac{1}{iK} + \frac{1}{0.62nFADo^{2/3}\omega^{1/2}\upsilon^{-1/6}Co} \tag{8}$$

The inverse kinetic current density, $1/i_k$, can be obtained from the intercept of Koutecky−Levich plot Figure 4. Reasonably linear plots are obtained (see the insets) at all measured potentials where ORR is expected to be under the mixed kinetics/diffusion control, and the linear plot under the pure diffusion control intercepts close to zero. Determination of i_k at different values of E allows determination of the standard rate constant $k°$ at different potentials where the rate of electron transfer is sufficiently slow (equilibrium) to act as a limiting factor and when the electron transfer is rapid in the limiting-current region. Standard rate constants varied from 3.8×10^{-2} to 4×10^{-3} cm^{-1} and 3×10^{-3} to 6×10^{-4} cm^{-1} for DMSO and MeCN, respectively. We can describe the ORR mechanism in $TBAPF_6$ solutions according to the reactions in Scheme 1, involving a one electron reduction of oxygen to superoxide (O_2^-) and subsequent reoxidation of superoxide to oxygen. An explanation for the reversible O_2 reduction process in TBA salt solutions and the superior stability of the superoxide, O_2^-, in the presence of TBA^+ in the various solvents is presented later in this paper.

SCHEME 1

Cathodic (E_{pc}): $O_2 + TBA^+ + e^- = TBAO_2$ (9)

Anodic (E_{pa}): $TBAO_2 - e^- = TBA^+ + O_2$ (10)

3.2. ORR in $LiPF_6$ Solutions in DMSO, DME, MeCN, and TEGDME. The ORR results obtained in these electrolytes will show clearly that the O_2 reduction mechanism in Li^+-containing electrolytes is different from that seen in presence of TBA^+. In addition, these results will demonstrate the subtle influence of the solvent on the mechanistic details of the O_2 reduction reactions in Li^+-containing electrolyte solutions as well as the rechargeability of the reduction products. We have found that the voltammetric data in DMSO is especially instructive to unambiguously map the O_2 reduction mechanism in Li^+-containing organic electrolytes relevant to the rechargeable Li−air battery.

Figure 5 illustrates O_2 reduction in 0.1 M $LiPF_6$/DMSO. This figure comprises four separate CVs overlaid. Each CV corresponds to a defined electrochemical window over which the voltammogram was scanned. The shortest window is shown in dark yellow (2.57−4.5 V) in which the scan was reversed at the half-peak potential $E_{pc1/2}$ (2.57 V) of the first cathodic peak to examine the associated anodic features. Reversing the sweep at $E_{pc1/2}$ resulted in two clear anodic peaks, E_{pa1} at 2.75 V followed by a broad peak (E_{pa2}) at 3 V. Expanding the cathodic scan to the peak potential E_{pc1} (2.45 V) produces an increase of the current in the following anodic E_{pa1} and E_{pa2} peaks becoming similar in magnitude. Two anodic peaks resulting from a single cathodic peak suggests a dual step reduction mechanism from the very beginning. A one-electron reversible process is characterized by the 56 mV difference between the cathodic peak and half-peak potential. For this system the potentials ($|E_{pc1} - E_{pc1/2}|$) are separated by 100 mV, demonstrating the complexity of this process. Upon scanning cathodically further, the current slope changes at 2.12 V, E_{pc2} (blue), signifying another electrochemical event. Reversing the scan subsequently in the positive direction results in the disappearance of E_{pa1} and increase in E_{pa2} peak current. This suggests that the first reduction product is consumed and converted to the second reduction product, which is oxidized at E_{pa2}. Finally, the cathodic sweep was allowed to continue toward 1.35 V (red line) where it was reversed. The corresponding anodic scan consists of two broad overlapping peaks. Similar to the blue scan E_{pa1} is absent and the magnitude of E_{pa2} decreased. The new anodic peak E_{pa3} that emerged is believed to be due to the oxidation of the product formed from the reduction at E_{pc2}.

As these reactions are irreversible, Randles−Sevcik and Levich treatments cannot be applied to these CV data. We have deconvoluted the data using the Nicholson and Shain relatioship[20] (eq 11) developed for irreversible electrochemical reactions,

$$I_p = (2.99 \times 10^5) n(n\alpha)^{1/2} A C D^{1/2} V^{1/2} \quad (11)$$

The symbols in eq 11 have their usual meaning. Figure 6a clearly shows that the number (n) of electrons transferred in the first reduction reaction is one since the theoretical $n = 1$, plot follows the experimental data. The best theoretical fit was obtained using a transfer coefficient $\alpha = 0.5$, which is a typical value for reversible reactions. This suggests that the first one-electron reduction of O_2 in DMSO/$LiPF_6$ is substantially reversible. Tafel analysis can also be used to obtain further insight. Tafel plots for ORR in 0.1 M $LiPF_6$/DMSO (from the CV data from figure 5) are depicted in Figure 6b. At low overpotentials between about 50 and 150 mV from OCP, the Tafel slope is close to 120 mV/dec. On the other hand, at high overpotentials, the value is approximately 220 mV/dec. A 120 mV/dec Tafel slope is typical of a one-electron process. The subsequent 220 mV/dec Tafel slope is due to a second reduction step. The observations in DMSO/$LiPF_6$ can be summarized by the reactions in Scheme 2 involving the formation of superoxide, O_2^- first (eq 12) which decomposes (eq 13), or is reduced further (eq 14), to form O_2^{2-}. Finally, O^{2-} is formed (eq 15) as the final reduction product O_2.

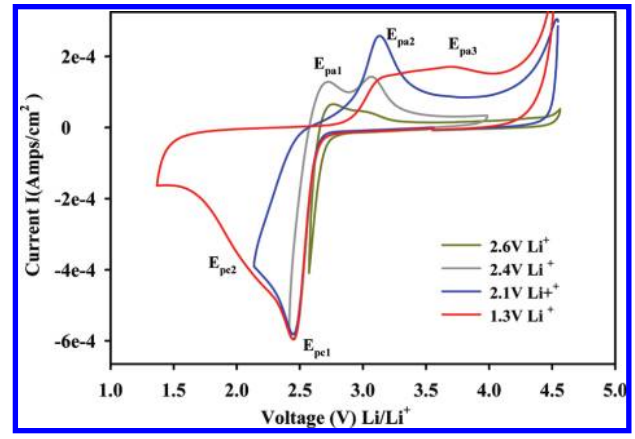

Figure 5. Cyclic voltammograms (*iR* corrected) for the reduction of oxygen in 0.1 M $LiPF_6$/DMSO at various potential windows. All scans used a glassy carbon working electrode. Scan rate of 100 mV/s.

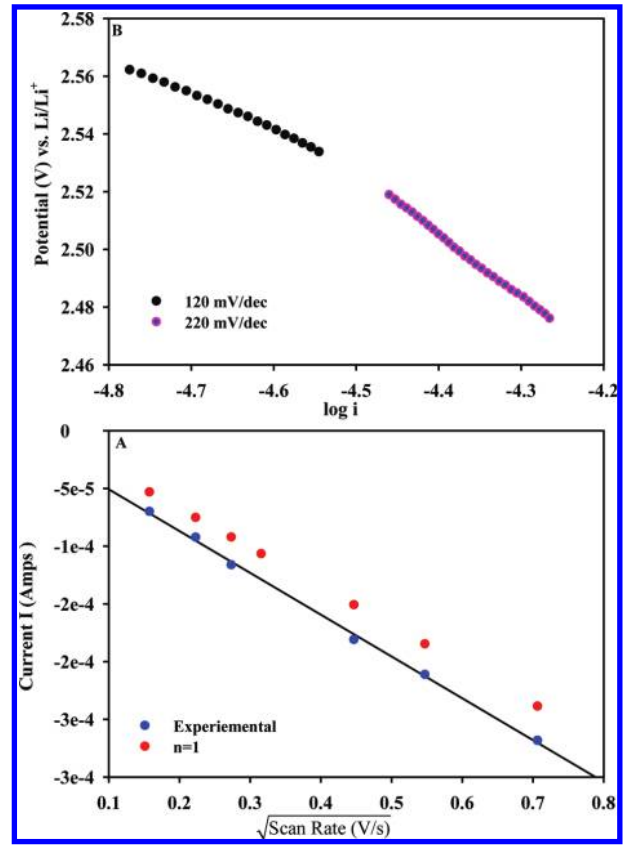

Figure 6. (A) Peak current vs square root of the scan rate in 0.1 M $LiPF_6$/DMSO. (B) Cathodic Tafel plot obtained in 0.1 M $LiPF_6$/DMSO during ORR. Scan rate = 10 mV/s.

SCHEME 2

Cathodic

$$O_2 + Li^+ + e^- = LiO_2 \quad (E_{pc1}) \qquad (12)$$

$$2LiO_2 = Li_2O_2 + O_2 \quad \text{(chemical)} \qquad (13)$$

$$LiO_2 + Li^+ + e^- = Li_2O_2 \quad (E_{pc2}) \qquad (14)$$

$$Li_2O_2 + 2Li^+ + 2e^- = 2Li_2O \quad (E_{pc3}) \qquad (15)$$

Anodic

$$LiO_2^- = O_2 + Li^+ + e^- \quad (E_{pa1}) \qquad (16)$$

$$Li_2O_2 = O_2 + 2Li^+ + 2e^- \quad (E_{pa2}) \qquad (17)$$

$$Li_2O = \frac{1}{2}O_2 + 2Li^+ + 2e^- \quad (E_{pa3}) \qquad (18)$$

Li_2O_2 as a discharge product of the Li−air battery is well recognized from Raman spectral analysis of discharged cathodes. Our recent unpublished X-ray diffraction data for discharged cathodes indicate that Li_2O_2 and probably Li_2O are discharge products of the Li−air battery. The anodic Tafel slope for E_{pa1} was calculated to be 128 mV/dec, which is quite similar to E_{pc1}, illustrating the reversibility of the first one-electron process. The corresponding apparent transfer coefficients (α) can be calculated from the Tafel slopes. The sum of $\alpha_c + \alpha_a = 1$, indicating that the number of electrons transferred between E_{pc1} and E_{pa1} is one. The kinetic parameters, the cathodic Tafel slope, the cathodic transfer coefficient (α_c), the number of electron transferred (n), and the exchange current density (i_o) are listed in Table 5. We note here that a reversible reduction of O_2 in a Li^+-containing electrolyte is reported here for the first time. The cyclic voltammetric parameters for the solutions of 0.1 M NBu_4PF_6 and $LiPF_6$ in dimethyl sulfoxide (DMSO), acetonitrile (MeCN), 1,2-dimethoxyethane (DME), and tetraethylene glycol dimethyl ether (TEGDME) are summarized in Table 3. A key difference between O_2 reduction in $LiPF_6$-containing DME, MeCN, or TEGDME solution and that in DMSO is the absence of E_{pc1} and the corresponding E_{pa1}. Single broad reduction and oxidation peaks are observed in the DME, MeCN, or TEGDME solutions, indicating multiple processes are occurring. We found E_{pc} shifts toward more negative potentials according to the order TEGDME < DME < MeCN < DMSO, indicating that the reduction of oxygen is hindered going from DMSO to TEGDME. The reduction of O_2 in acetonitrile/$LiPF_6$ is shown in Figure 7. The cathodic peak and half-peak potential are separated ($|E_{pc} - E_{pc/2}|$) by 220 mV, indicating a complex reduction mechanism. Examining the complete CV, we notice a large broad oxidation peak at 3.33 V. We studied anodic processes as a function of cathodic sweep reversal potentials. The CV is first scanned to 2.5 V, which is just after the reduction onset potential. There is little anodic activity at this potential. The lack of anodic activity indicates that the initial reduction step is irreversible or that the product undergoes a secondary reaction like that eq 13 in Scheme 2. When the electrochemical window is increased to 2.37 V, the half-wave potential ($E_{pc/2}$) produces an anodic response E_{pa2} at 3.25 V (gray line), which, on the basis of the DMSO data and our previous results in acetonitrile, is believed to be the oxidation of Li_2O_2. This suggests that Li_2O_2 is formed

TABLE 3: Voltammetric Properties of Oxygen Saturated Electrolytes (Scan Rate 100 mV/s)

electrolyte	E_{pc}(V)	E_{pa}(V)	E_{pa2}(V)	ΔE_p(V)	E° (V)
$DMSO^{Li+}$	2.54	2.77	3.17	0.23	2.65
$DMSO^{TBA+}$	2.34	2.40		0.06	2.37
$MeCN^{Li+}$	2.32	3.33		1.01	
DME^{Li+}	2.05	3.26		1.21	
$TEGDME^{Li+}$	1.76	2.98		1.22	

at E_{pc} via the reactions in eqs 13 and 14. Anodic peak capacity increases as the electrode is swept cathodically, closer to the peak potential of 2.27 V (E_{pc}). Maximum anodic activity is reached after sweep reversal at 2.10 V, a potential just after E_{pc}. E_{pa2} begins to broaden and a second anodic peak E_{pa3} emerges as the potential is scanned cathodically to 1.65 V. The presence of this second anodic peak suggests a third reduction process occurs as the electrode is cathodically polarized to low potentials, possibly the reduction of Li_2O_2 to Li_2O, eq 15. Scanning the electrode to 0.65 V results in disappearance of E_{pa2} in the following anodic scan. Oxygen reduction CVs in $LiPF_6$/DME and $LiPF_6$/TEGDME are illustrated in Figure 8a,b, respectively. The cathodic peaks are shifted negatively relative to MeCN, attributed to an increase in solution resistance and the associated *iR* polarization. Little anodic activity is visible prior to arriving at the half-wave reduction peak potential $E_{pc/2}$. The anodic peaks continue to broaden as the CV is scanned toward E_{pc}. The broadness of the anodic peak with increasing cathodic potentials indicates that more than one reduction reaction occurs. The oxidations of these reduction products occur at E_{pa1}, E_{pa2}, and E_{pa3}. We see that DME and TEGDME differ in that E_{pa2} in DME is the predominant peak, while E_{pa3} manifests itself as the dominant anodic peak in TEGDME, once the electrode is polarized below E_{pc}. We interpret these results to mean that the LiO_2 formed in the ether electrolytes decomposes rapidly to Li_2O_2, as we observed in MeCN, and that the Li_2O_2 is readily reduced to Li_2O.

Figure 9a shows both a Randles−Sevcik plot for a reversible redox couple (for $TBAPF_6$) and a Nicholson plot for an irreversible couple (for $LiPF_6$) in MeCN. Note the large difference in current for ORR in this electrolyte. A combination of electrode passivation, oxygen solubility, and transfer coefficient contribute to the decrease of current. The diffusion coefficients of oxygen in both electrolytes are presented in Table 4. Figure 9b shows the scan rate dependence of ORR in both DME and TEGDME based electrolytes. These plots display an

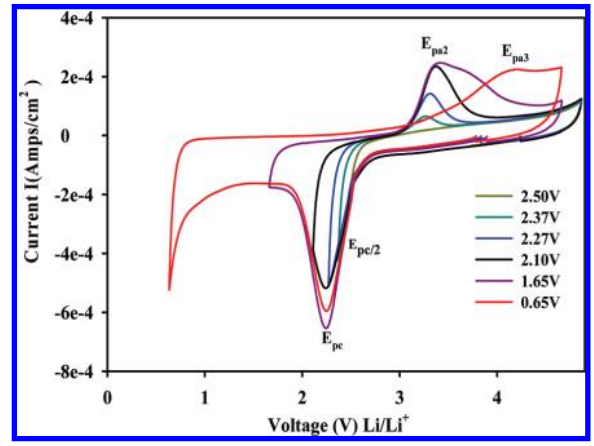

Figure 7. Cyclic voltammograms (*iR* corrected) for the reduction of oxygen in 0.1 M $LiPF_6$/MeCN at various potential windows. All scans used a glassy carbon working electrode. Scan rate of 100 mV/s.

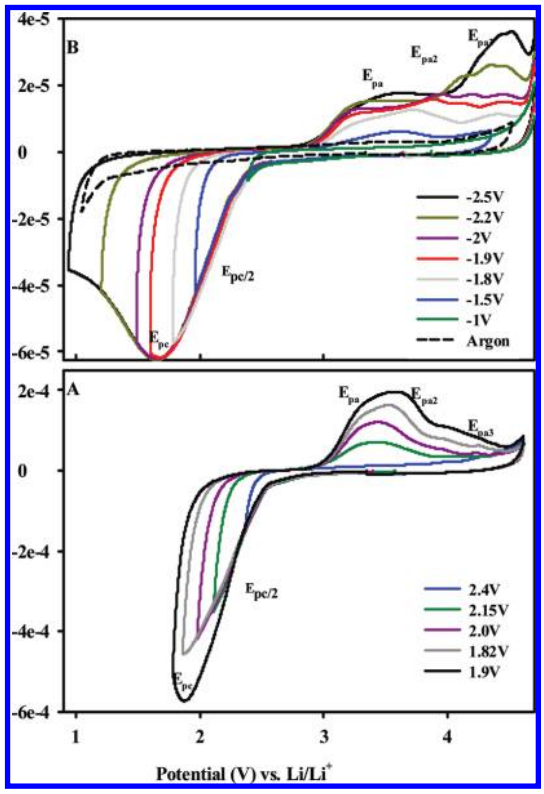

Figure 8. Cyclic voltammograms (*iR* corrected) for the reduction of oxygen in (A) 0.1 M $LiPF_6$/DME and (B) 0.1 M $LiPF_6$/TEGDME at various potential l windows. All scans used a glassy carbon working electrode. Scan rate of 100 mV/s.

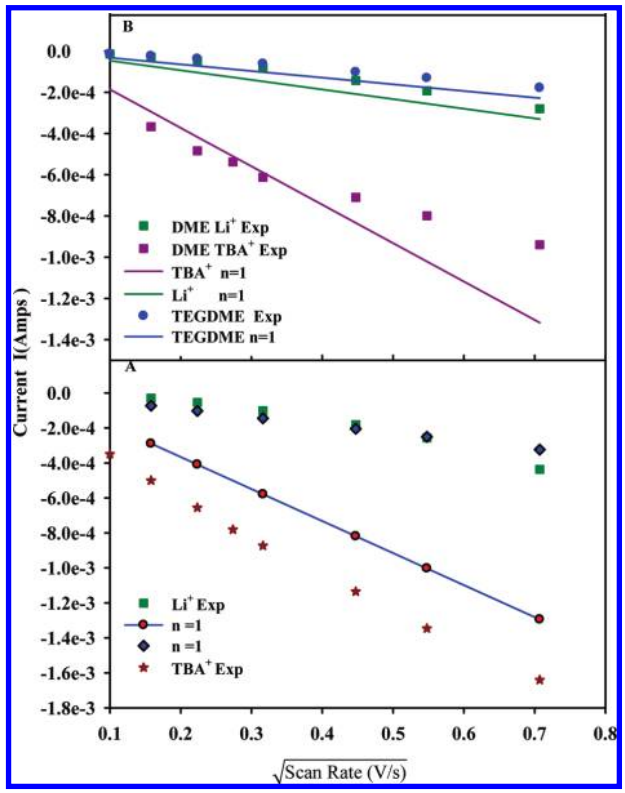

Figure 9. Peak current vs square root of the scan rate plots for the reduction of oxygen in (A) 0.1 M $TBAPF_6$ and 0.1 M $LiPF_6$/MeCN (n = number of e^-) and (B) 0.1 M TBA^+ and $LiPF_6$/DME and 0.1 M $LiPF_6$/TEGDME on a GC electrode.

obvious linear relationship between peak current and scan rate. Both plots clearly obey the Nicholson equation, demonstrating

TABLE 4: Oxygen Diffusion Coefficient in Electrolytes

solvent	diffusion coefficient (cm^2/s)
$DMSO^{Li+}$	1.67×10^{-5}
$DMSO^{TBA+}$	9.75×10^{-6}
$MeCN^{Li+}$	4.64×10^{-6}
$MeCN^{TBA+}$	2.45×10^{-5}
DME^{Li+}	1.22×10^{-5}
DME^{TBA+}	3.88×10^{-6}
$TEGDME^{Li+}$	2.17×10^{-6}

that the oxygen reduction process is totally irreversible in these electrolytes. This is consistent with the rather small exchange current values derived below. Cathodic current generated by ORR in the presence of TBA^+ is an order of magnitude larger than the Li^+ based electrolyte. Plots of experimental data follow theoretical $n = 1$ plots quite well although not to the same extent as in DMSO. The Tafel slopes are much higher, as is the case for MeCN (484 mV/dec). As the mixed potential region dominates, it is difficult to extract precise kinetic values from these Tafel plots. In such cases it is useful to apply electrochemical impedance spectroscopy (EIS).

3.3. Impedance Spectroscopy To Determine O_2 Reduction Kinetics. Reaction kinetics can be discerned from Faradaic impedance experiments when the working electrode's potential is held at equilibrium. Departure from equilibrium can be characterized by the linearized relationship written in terms of the electronic current as

$$R_s - \frac{1}{\omega C_s} = R_{ct} = \frac{RT}{Fi_o} \tag{19}$$

Using this equation, we can easily evaluate the exchange current, and therefore $k°$ (see eq 20), when the charge transfer resistance R_{ct} is known. Extrapolation of kinetic data close to the equilibrium potential is accomplished by comparing the calculated data with the experimental results. The data can be analyzed using an equivalent circuit in which the double layer capacitor is in series with the charge transfer resistance R_{ct}.[21] Z_{real} is plotted versus $\omega^{-1/2}$ in Figure 10, where Z_{real} is the real component of impedance series resistance and ω is frequency. The intercept of this plot is R_{ct}.[20] The exchange current i_o is determined from eq 19, and subsequently the standard rate constant $k°$ is calculated using eq 20.

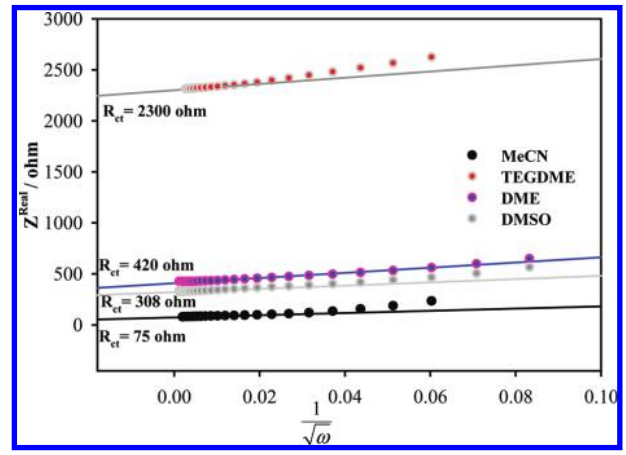

Figure 10. Real impedance versus inverse square root of frequency in 0.1 M $LiPF_6$ DMSO (gray), DME (blue), TEGDME (red), and MeCN (black).

$$i_o = nFAk^oC \quad (20)$$

The rate constant provides a true measure of reaction kinetics, and these values are tabulated in Table 5. Table 5 shows that the rate constant decreases as the solvents DN decreases. This dependence implies that the kinetics of the reaction is influenced strongly by solvent.

3.4. Understanding ORR in Nonaqueous Electrolytes Using Pearson's HSAB Theory. Pearson's hard soft acid base (HSAB) theory[22] states that hard acids prefer hard bases and soft bases prefer soft acids. The ions present in the solutions used in this study are the supporting electrolyte ions TBA^+, PF_6^-, and Li^+ and the electrochemically generated ions superoxide (O_2^-), peroxide (O_2^{2-}), and monoxide (O^{2-}). The TBA^+ is classified as a soft acid due to its large radius of 0.494 nm (in DMSO)[23] and low charge density. It has been shown that tetraalkylammonium ions, NR_4^+, are poorly solvated[24,25] in organic electrolytes due to their large size and the small surface charge. A solvent's basicity is usually characterized by its donor number (DN), which for the solvents used here follows the order MeCN(14.1) < TEGDME(16.6) < DME(20.0) < DMSO(29.8). Solvent acidity can be characterized by its acceptor number (AN), which in these solvents follows the order DME(10.2) < TEGDME(10.5) < MeCN(18.9) < DMSO(19.3). In TBA/DMSO electrolytes, although DMSO has a high DN, TBA^+ is weakly solvated. Consequently, solvent−TBA^+ interactions are weak in the electrolytes, allowing TBA^+ to roam more or less as a naked ion.[26] Among the oxides formed from the reduction of oxygen, O_2^- has a relatively large radius and low charge density, which makes it a moderately soft base. In keeping with the HASB theory, the naked soft acid TBA^+ stabilizes the soft base O_2^- in the electrolyte with the formation of an ion pair complex of the type I (Chart 1).

Reversibility of the O_2/O_2^- redox couple in TBA^+ solutions is a result of this stable solution species I. As O_2^- is strongly coordinated to TBA^+ in I, further reduction of superoxide to peroxide (O_2^{2-}) is hindered. The reversibility trend observed in Figure 1B appears to follow the acceptor number (AN) trend as the AN increases PF_6^-−solvent interactions also increase, providing even more TBA^+ to interact with O_2^-. Thus, DMSO exhibits excellent electrochemical reversibility for the O_2/O_2^- couple. The lower current in the CV of O_2 in DMSO as compared to that for DME and ACN is probably due to its lower oxygen solubility. Acetonitrile with high oxygen solubility yields a high current for O_2 reduction and excellent reversibility in the presence of TBA^+. In the case of DME $TBAPF_6$ solutions, both the anodic and cathodic peaks in the CV are separated by almost one volt, indicative of slow kinetics.

According to the HSAB theory, alkali metal ions are hard Lewis acids and have a high affinity for hard Lewis bases such as the peroxide and monoxide formed from the reduction of O_2. In electrolyte solutions, the hard Lewis acid Li^+ ions are solvated by the solvents, usually by about four solvent molecules per Li^+ to form solvent separated ion pairs, for example, $Li^+(DMSO)_4PF_6^-$ in DMSO solutions. The Li^+−solvent bond strength in the complexes would follow the solvent DN scale as DMSO > MeCN > DME > TEGDME. Nuclear magnetic resonance studies have revealed that these solvated ion pairs are fluxional complexes even down to −20 °C. Although Li^+ behaves as a hard acid, its acidity is modulated (or more precisely lowered) by the strength of the coordination bonds in Li^+−$(solvent)_n$ formed with the solvent.[27] Since superoxide is a moderately soft base, it has a low affinity for the hard acid Li^+ present in Li^+-conducting electrolytes. Consequently, the superoxide formed as the first reduction product of O_2 will want either to decompose or to undergo a fast second reduction to form the hard base, peroxide (O_2^{2-}), as shown in eqs 13 and 14.

Peroxide is a strong Lewis base that wants to be associated with the strong base Li^+. Similarly, the ultimate reduction product of O_2, the monoxide O^{2-}, is a hard base with a strong affinity for Li^+. Consequently, based on the HSAB theory, the stable O_2 reduction products in the Li ion containing electrolyte solutions are Li_2O_2 and Li_2O.

As mentioned above, the formation of the Li^+−$(solvent)_n$ complexes would lower the acidity of Li^+, roughly in proportion to the donor number of the solvent.

In DMSO solutions of $LiPF_6$, the Li^+ Lewis acidity is decreased more than in other solvents due to its higher DN. As a result, the superoxide, O_2^-, formed as the first O_2 reduction product has an increased affinity for these solvated Li^+, the O_2^- is stabilized longer in solution, in a structure of the type II (Chart 2), reminiscent of the TBA^+---O_2 complex I.

This explains the distinct O_2/O_2^- couple seen in the DMSO/$LiPF_6$ solutions. Our results suggest that depending on the basicity of the solvent measured by its DN, the superoxide formed as the first reduction product of oxygen will be stabilized to varying degrees before transformation to O_2^{2-} via a chemical or an electrochemical reaction. The multistep electrochemical reduction of O_2 in Li^+-containing electrolyte solutions can be schematically represented in Scheme 3.

High DN solvents provide increased stability for complex II because of the modulated, or more precisely decreased, Lewis acidity of the hard acid via complex II. In such electrolytes a distinct O_2/O_2^- reversible couple may be seen in the presence of Li^+. In solvents with low DN, the general tendency is for

TABLE 5: O_2/O_2^- Kinetic Parameters of 0.1 M Li and $TBAPF_6$

solvent	R_{ct}	Tafel (E_{pc}):(E_{pc2}) (mV/dec)	Tafel (E_{pa}):(E_{pa2}) (mV/dec)	α_{rds}	k° (cms^{-1})
$DMSO^{Li+}$	308	123:220	129:400	0.5	2.10×10^{-4}
$DMSO^{TBA+}$	400	120	120	0.5	1.7×10^{-2}
$MeCN^{Li+}$	75	484:209	331		2.10×10^{-4}
DME^{Li+}	420	360:388	243		1.58×10^{-4}
$TEGDME^{Li+}$	2300	304:660	243		1.11×10^{-5}

CHART 1: Structure I: Ion Pair between TBA^+ and O_2^- [a]

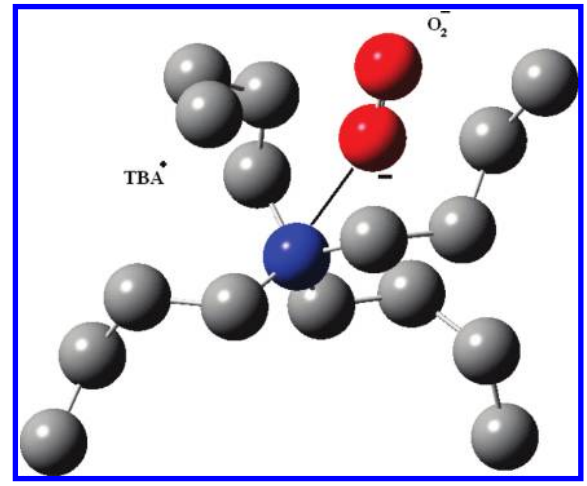

[a] Nitrogen is blue, carbon is gray, and O is red. Alkyl hydrogens are omitted in the structure.

CHART 2: Structure II: Ion Pair between Solvated Li^+ and O_2^{-a}

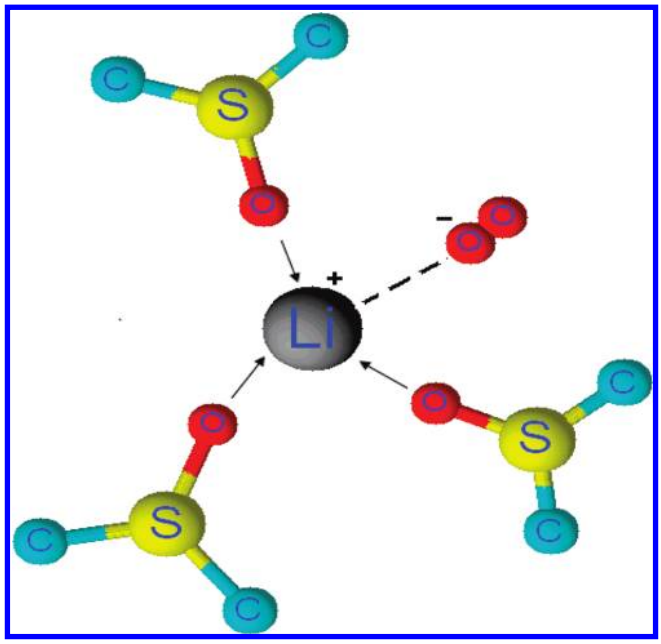

[a] The methyl hydrogens are omitted in the structure.

SCHEME 3

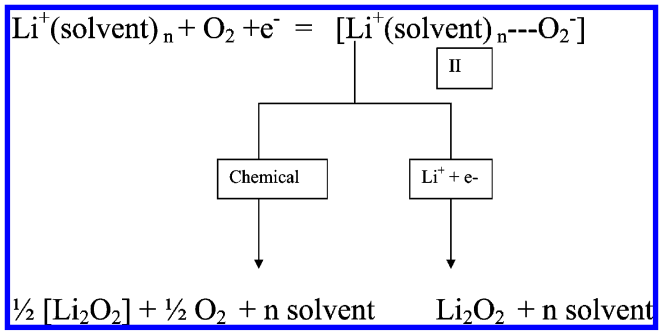

the O_2^- to quickly decompose or to undergo fast electrochemical reduction to O_2^{2-} and further to O^{2-}.

4. Conclusions

Aprotic nonaqueous organic solvents were investigated to determine their influence on the ORR reactions relevant to the rechargeable Li−air battery. We have determined how the supporting electrolyte cations, TBA^+ and Li^+, together with the solvents comprising the electrolyte solutions influence the nature of reduction products. In solutions containing TBA^+, O_2 reduction is a highly reversible one-electron process involving the O_2/O_2^- couple. On the other hand, in Li^+-containing electrolytes relevant to the Li−air battery, O_2 reduction proceeds in a stepwise fashion to form O_2^-, O_2^{2-}, and O^{2-} as products. These reactions in the presence of Li^+ are kinetically irreversible or quasi-reversible. The stabilization of the one-electron reduction product, superoxide (O_2^-), in TBA^+ solutions in all of the solvents examined can be explained using Pearson's Hard Soft Acid Base (HSAB) theory through the formation of the TBA^+---O_2^- complex. The HSAB theory coupled with the relative stabilities of the Li^+−$(solvent)_n$ complexes existing in the different solvents can also provide a rational explanation for the different O_2 reduction products formed in Li^+-conducting electrolyte solutions. High DN solvents provide increased stability for the complex $[Li^+(solvent)_n$---$O_2^-]$ because of the modulated Lewis acidity of the hard acid. In such electrolytes a distinct O_2/O_2^- reversible couple may be seen in the presence of Li^+. In solvents with low DN, the general tendency is for the O_2^- to quickly decompose or to undergo fast electrochemical reduction to O_2^{2-}. In Li^+ electrolytes prepared in low DN solvents O_2 may be fully reduced to O^{2-}.

Acknowledgment. U.S. Army CERDEC through Subcontract No. GTS-S-6-1-437 supported this work.

References and Notes

(1) Abraham, K. M.; Jiang, Z. *J. Electrochem. Soc.* **1996**, *143*, 1–5.
(2) Abraham, K. M.; Jiang, Z.; Carroll, B. *Chem. Mater.* **1997**, *9*, 1978–1988.
(3) O'Laoire, C.; Mukerjee, S.; Abraham, K. M.; Plichta, E. J.; Hendrickson, M. A. *J. Phys. Chem. C* **2009**, *113*, 20127–20134.
(4) Choe, H. S.; Carroll, B. G.; Pasquariello, D. M.; Abraham, K. M. *Chem. Mater.* **1997**, *9*, 369–379.
(5) Zhang, S. S.; Foster, D.; Read, J. *J. Power Sources*, *195*, **2010**, 1235−1240.
(6) Read, J. *J. Electrochem. Soc.* **2002**, *149*, A1190–A1195.
(7) Read, J. *J. Electrochem. Soc.* **2006**, *153*, A96–A100.
(8) Read, J.; Mutolo, K.; Ervin, M.; Behl, W.; Wolfenstine, J.; Driedger, A.; Foster, D. *J. Electrochem. Soc.* **2003**, *150*, A1351–A1356.
(9) Ye, H.; Xu, J. J. *ECS Trans.* **2008**, *3*, 73–81.
(10) Kuboki, T.; Okuyama, T.; Ohsaki, T.; Takami, N. *J. Power Sources* **2005**, *146*, 766–769.
(11) Xu, W.; Xiao, J.; Zhang, J.; Wang, D.; Zhang, J.-G. *J. Electrochem. Soc.* **2009**, *156*, A773–A779.
(12) Kumar, B.; Kumar, J.; Leese, R.; Fellner, J. P.; Rodrigues, S. J.; Abraham, K. M. *J. Electrochem. Soc.*, *157*, **2009**, A50−A54.
(13) Wang, Y.; Zhou, H. *J. Power Sources*, *195*, **2009**, 358−361.
(14) Beattie, S. D.; Manolescu, D. M.; Blair, S. L. *J. Electrochem. Soc.* **2009**, *156*, A44–A47.
(15) Débart, A.; Paterson, Allan J.; Bao, J.; Bruce, Peter G. *Angew. Chem., Int. Ed.* **2008**, *47*, 4521–4524.
(16) O'Laoire, C.; Abraham, K. M.; Mukerjee, S. *ECS Mtg. Abstr.* **2009**, *804*, 404.
(17) Gutmann, V. *Coord. Chem. Rev.* **1976**, *18*, 225–255.
(18) Sawyer, D. T.; Chiericato, G.; Angelis, C. T.; Nanni, E. J.; Tsuchiya, T. *Anal. Chem.* **1982**, *54*, 1720–1724.
(19) Tsushima, M.; Tokuda, K.; Ohsaka, T. *Anal. Chem.* **1994**, *66*, 4551–4556.
(20) Nicholson, R. S.; Shain, I. *Anal. Chem.* **1964**, *36*, 706–723.
(21) Bard, A. J. *Electrochemical Methods Fundamentals and Applications*, 2nd ed.; John Wiley & Sons: New York, 2001.
(22) Pearson, R. G. *J. Am. Chem. Soc.* **1963**, *85*, 3533–3539.
(23) Paul, R. C.; Johar, S. P.; Banait, J. S.; Narula, S. P. *J. Phys. Chem.* **1976**, *80*, 351–352.
(24) Gnanaraj, J. S.; Thompson, R. W.; DiCarlo, J. F.; Abraham, K. M. *J. Electrochem. Soc.* **2007**, *154*, A185–A191.
(25) Tsierkezos, N. G.; Philippopoulos, A. I. *Fluid Phase Equilib.* **2009**, *277*, 20–28.
(26) Frech, R.; Huang, W. *J. Solution Chem.* **1994**, *23*, 469–481.
(27) Abraham, K. M.; Pasquariello, D. M.; Martin, F. J. *J. Electrochem. Soc.* **1986**, *133*, 661–666.
(28) Goldfarb, D. L.; Longinotti, M. P.; Corti, H. R. *J. Solution Chem.* **2001**, *30*, 307–322.
(29) Rivas, M. A.; Iglesias, T. P.; Pereira, S. M.; Banerji, N. *J. Chem. Thermodyn.* **2006**, *38*, 245–256.
(30) Lago, A.; Rivas, M. A.; Legido, J.; Iglesias, T. P. *J.Chem. Thermodyn.* **2009**, *41*, 257–264.
(31) *Chemistry of Nonaqueous Solutions:Current Progress*; Mamantov, G., Ed.; Wiley: New York, 1994.
(32) Aminabhavi, T. M.; Gopalakrishna, B. *J. Chem. Eng. Data* **1995**, *40*, 856–861.
(33) Marcus, Y. *The Properties of Solvents*; Wiley: New York, 1998.

JP102019Y